SIMULTANEOUS FOCUSING AND CONTOURING OF HUMAN ZYGOTES FOR IN VITRO FERTILIZATION

Alessandro Giusti, Giorgio Corani, Luca Gambardella
Dalle Molle Institute for Artificial Intelligence, SUPSI and University of Lugano, Switzerland

Cristina Magli
International Institute for Reproductive Medicine, Lugano, Switzerland

Luca Gianaroli
INFERGEN, Lugano, Switzerland

Keywords: In vitro fertilization, Microscopy, Phase contrast, Hoffmann modulation contrast, Segmentation, Contouring, Autofocus.

Abstract: Observation of ovocytes and zygotes plays an important role in In Vitro Fertilization procedures, and is usually perfomed by means of a microscope equipped with Hoffman Modulation Contrast optics, which produces images with a complex, side-lit, 3D-like appearance. Our algorithm operates on a Z-stack of such images taken at different focal planes, and simultaneously identifies: a) a repeatable, meaningful focal plane corresponding to the cell's equator line, and b) the external contour of the cell. As the cell is a thick stucture with respect to the microscope depth of field, the two problems are nontrivial and deeply related. Our algorithm is also robust to other structures, clutter and artefacts affecting the images and lying at varying focal planes. We describe implementation details, applications and experimental results of our technique.

1 INTRODUCTION

During In Vitro Fertilization (IVF) procedures, biologists observe zygotes (fertilized ova) at different times in order to assess their quality and select the ones maximizing the implantation success rate (Gianaroli et al., 2007). Such observations are usually performed by means of an inverted microscope with Hoffmann Modulation Contrast and 20x or 40x magnification, where focusing plays an important role as the depth of field is quite shallow, so that only a thin slice of the cell's volume is clearly visible at a single focal plane. We solve the problem of automatically finding a repeatable and sensible focal plane from a set of images taken at different focal planes (Z-stack), by means of an original approach where high-level scene information (the cell contour) is recovered simultaneously with the correct focal plane (see Figures 1 and 2).

Traditional autofocusing algorithms based on global or local contrast fail at consistently finding a meaningful and repeatable focus for the zygote observation: in fact, many images in a Z-stack exhibit sharp, strong-contrast features. Structures of interest such as pronuclei and polar bodies can be found at different depths, and therefore come into focus at different levels (see Figure 1); a number of other structures, such as fragments and debris, are also visible at varying depths, both inside and outside the cell, representing strong and confusing clutter for automated processing.

We maintain that a proper solution to the focusing problem requires an higher-level understanding of the scene. Our approach is therefore aimed at solving both of the following problems:

- segment the zygote cell, and
- find a focal plane where the sharpness of its contour is maximized, which roughly corresponds to the plane of the cell's contour generator curve.

The two tasks are deeply related: in fact, the cell's actual contour can only be recovered in an image where it is sharply visible, and such image can only be easily determined when the contour itself is known.

We solve both problems simultaneously by representing data from all focal planes in a single graph,

Giusti A., Corani G., Gambardella L., Magli C. and Gianaroli L. (2010).
SIMULTANEOUS FOCUSING AND CONTOURING OF HUMAN ZYGOTES FOR IN VITRO FERTILIZATION.
In *Proceedings of the Third International Conference on Bio-inspired Systems and Signal Processing*, pages 151-158
DOI: 10.5220/0002592501510158

(a) I_1 (b) I_6 (c) I_{14} (d) I_{19} (e) I_{23}

Figure 1: The source stack is composed by a number of images (slices) taken at different focus levels. Our experiments use 23-slice stacks; 5 slices covering the whole range of a typical stack are shown in the figure. Note in-focus debris generating strong contrast in (d,e), whereas the best focus of the cell is in (c).

then solving a minimum-cost path problem on such graph. Sharp, in-focus edges are favored by assigning a lower cost to localized, large gradient magnitudes. We also take advantage of the complex, 3D-like sidelit appearance of the zygote in HMC images for improving the system's robustness, by enforcing priors about the cell lighting, which is a predictable and prominent feature. Finally, the peculiar topology of the graph on which the minimum-cost path problem is solved implicitly enforces:

- shape priors on the cell contour, which is expected to be smooth and circular-shaped;
- limited and smooth variations in focus along the contour.

A similar approach has been used for robust zygote segmentation from a single image in (Giusti et al., 2009), where the cell is assumed to be already correctly focused, which implies manual intervention in the image acquisition process.

On the contrary, our approach removes any influence of the operator in the focusing process; this is especially important as the focal plane found by our algorithm roughly bisects the cell in a top and bottom half. This acts as an important reference for determining the relative position of other structures of interest. In addition, the knowledge of the zygote contour is useful to readily compute a number of quantitative measures (apparent size, simple shape descriptors, relative positions) for the cell, which are not easily judged otherwise. The obtained segmentation and focal plane may also be applied for other tasks, such as driving an automated microscope for unattended imaging of zygotes, or providing a robust, precise initialization for subsequent (automatic or user-assisted) analysis algorithms, such as those introduced in (Morales et al., 2008; Karlsson et al., 2005) for the segmentation of the zona pellucida.

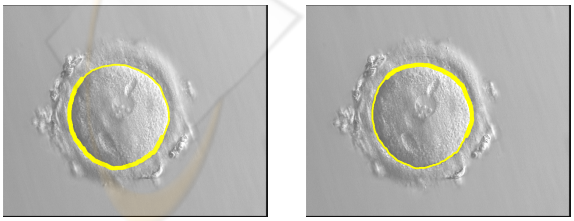

(a) I_{13} (b) I_{14}

Figure 2: Results for the stack in Figure 1. Our algorithm detects the contour γ of the zygote (yellow line). It is best focused (thick line) partly in I_{13} (lower-left part) and partly I_{14} (upper-right segment).

We briefly review related works in the following Section, then introduce notation and terminology in Section 3. Our approach is then described in detail in section 4, and experimentally validated in in Section 5. Section 6 concludes the paper and presents ongoing work.

2 RELATED WORKS

Autofocus systems are widely used in microscopy, and can be implemented either by means of additional hardware, or by using a software approach for analyzing a sequence of camera images taken at varying focus positions; our system belongs to the latter category. Many approaches for software autofocus are documented in literature (Shih, 2007), mostly based on the maximization of local or global contrast: the core difference of our approach is that we seek an higher level understanding of the scene, thus providing a repeatable focusing position which is linked to a specific focal plane which bisects the cell in a top and bottom half. As the sample is thick with respect to the depth of field, and many other sources of contrast exist in different focal planes, the same goal can not be attained by a lower level analysis.

Our approach is based on the segmentation of the cell contour, which by itself is not a straightforward task even if the correct focal plane was known, due to the complexity of the image.

Classical region-based segmentation algorithms, including watersheds (Soille and Vincent, 1991), are

not applicable in this context because of the complex appearance of the cell, including the surrounding zona pellucida, clutter, and artifacts; this also hinders the application of straightforward edge-based segmentation algorithms, as many spurious contours are detected.

Iterative energy minimization methods such as active contours (Xu, 1998) and level sets are frequently employed in biomedical imaging: in this context, their application is not straightforward because debris are likely to generate several local minima in the energy function, which makes quick and robust convergence problematic; for example, in (Morales et al., 2008) active contours are used for measuring the thickness of the zona pellucida in embryo images, but only after a preprocessing step aimed at removing debris and other artifacts.

In (Beuchat et al., 2008) a semisupervised technique for measuring various zygote features is used, where the cell shape is approximated by an ellipse: in our case, instead, we recover the actual shape of the cell, which is often not well approximated by an ellipse.

The technique we are presenting includes a global energy minimization step, and may be classified as a specialized graph-cut (Zabih and Kolmogorov, 2004) approach, where: *a)* priors on the cell shape are accounted for by operating on a spatially-transformed image and searching for a minimum-cost path on a directed acyclic graph; *b)* priors on the contour appearance due to HMC lighting are directly integrated in the energy terms; *c)* information at different focal planes is simultaneously represented in a single large graph. We are therefore extending the approach in (Giusti et al., 2009) by operating on information from many focal planes at the same time.

Interestingly, several previous works handled the peculiar lighting in HMC and DIC images as an obstacle to segmentation (Kuijper and Heise, 2008), and adopted preprocessing techniques for removing it, whereas we actually exploit such appearance for improving robustness.

3 PRELIMINARIES, MODEL AND NOTATION

Our algorithm is designed to operate on a Z-stack of N images taken with Hoffman Modulation Contrast (HMC) microscopy[1]. We denote the input images as $I_1, I_2, ..., I_N$, and their respective focal planes $z = z_1, z_2..z_N$. Such focal planes can be considered horizontal slices at different depths of a 3D space whose cartesian axes are (x, y, z).

HMC is an imaging technique converting optical slopes to variations of the light intensity: it is routinely used in IVF labs for observing zygotes, as it provides a large amount of contrast for transparent specimens and eases human observation as the objects appear three-dimensional and side-lit, as if a light source was illuminating them from a side (apparent lighting direction).

The underlying imaging model is considerably complex, especially if the effect of out-of-focus features is taken into account. Still, several intuitive principles hold, on which we base our approach:

- structures which lie on or near the current focal plane z_i appear sharp and exhibit strong localized gradients in the image intensity I_i;
- as the focal plane depth moves farther from the structure's depth, the structure image becomes blurred. Consequently, its gradients of the structure's image lose locality and strength, although the *global* contrast and visibility of the feature may not be affected, or may even be emphatised in some situations[2].

In this work, the main feature of interest is the cell contour; as the cell is a 3D object, in order to explain the appearance of its contour at different focus levels, we provide the following formalization: Let S be the surface of the cell, which we assume to be smooth, in the 3D space (x, y, z). The contour generator curve Γ is a curve in 3D space, identified by the locus of points P on S such that the tangent plane to S in P contains the z direction[3]. Although this definition allows Γ to be composed by several disjoint curve parts, the regularity of the cell shape, which is convex and ellipsoid-like, allows us to assume that Γ is a single, closed curve in the following.

We are interested in detecting the image of the contour generator curve Γ in our input images I_i. In particular, let γ be the 2D apparent contour, i.e. the orthogonal projection of Γ on the (x, y) plane. Following the principles introduced previously in this section, a part of γ is visible and well-focused in an image I_i if the corresponding part of Γ is on or near the $z = z_i$

[1] a technique delivering visually similar results is Differential Interference Contrast (DIC), which is also a likely application scenario for our technique.

[2] in fact, a slightly defocused feature imaged through a phase contrast technique may appear more evident to an human operator than the same feature in perfect focus; this makes manual focusing inherently operator-dependent and hardly repeatable.

[3] Note that this is similar to the concept of contour generator curve in projective geometry where an ortographic camera is considered.

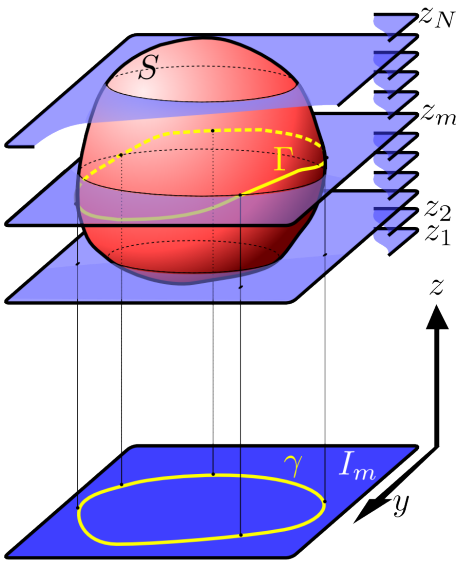

Figure 3: Representation of model (see text).

plane; in this case, such part of γ will exhibit large, localized gradients in image I_i. The gradient intensity is weaker as Γ gets farther away from the plane $z = z_i$; eventually, if a part of Γ lies far from the plane $z = z_i$, then the corresponding part of γ may be invisible (i.e. not generating any significant gradient) in I_i.

Our goal is to identify γ in the (x,y) image coordinates, as well as the I_m image where γ is most visible, whose focal plane z_m corresponds to the depth of Γ. As described in the following Section, we account for the fact that different parts of Γ may lie at different depths, by detecting different parts of γ on different I_i images.

4 SIMULTANEOUS FOCUSING AND CONTOURING OF A ZYGOTE CELL

We divide the segmentation process in two sequential steps: first, we find the approximate location $(x,y) = (c_x,c_y)$ of the cell center; in doing this, we assume that a single zygote is visible in the image, which is always the case as zygotes are kept in separate wells in clinical practice.

Then, we build a transformed representation of the whole Z-stack in polar coordinates, constructing a single graph, then using a minimum-cost path formulation in order to recover the actual zygote contour and its focus plane.

We briefly introduce the former part, which we consider of lesser importance and interest, in Section 4.1. The main focus is instead on the latter part, described in Section 4.2.

4.1 Approximate Localization of Zygote Center

First, a representative image for the whole stack is selected, by applying a naive autofocusing algorithm: in particular, for each slice i we compute a number $f(i)$ as the average value for the modulo of the gradient of I_i. We consider the slice b maximizing such value:

$$b = \operatorname*{argmax}_i (f(i)). \quad (1)$$

Due to the gradient in the internal part of the cell, and strong gradients due to debris and additional structures, I_b does not represent in general the slice where γ is most visible (see Section 5). However, it proves to be a suitable image for applying the same algorithm described in (Giusti et al., 2009) for roughly detecting the cell centroid.

In particular, in order to find an approximate location for the cell centroid, the modulo of the image gradient of I_b is subsampled to a smaller image, which is automatically thresholded then regularized by means of median filtering (see Figure 4 a,b). The largest connected component is isolated and its holes filled (Figure 4 c); for each point inside the resulting region, the minimum distance to the region boundary is computed by means of the distance transform; the point with the maximum distance is finally chosen as the approximate centroid of the cell.

This preliminary analysis phase is not critical for the quality of results, as the subsequent processing tolerates quite large displacements of the detected centroid; nonetheless, this simple algo- rithm counterintuitively proves to be quite robust also in presence of large artifacts attached to the cell; this is mainly due to the distance transform, which implicitly cancels or reduces the effect of any non-convex artifact protruding of the border of the cell.

4.2 Contouring and Focusing of the Zygote

4.2.1 Transformation to Polar Coordinates

Once the zygote centroid (c_x,c_y) is detected in one slice, it is considered valid in all the images of the stack (as no significant displacements happens between focus levels). For each image I_i, a circular corona centered at such point is transformed using

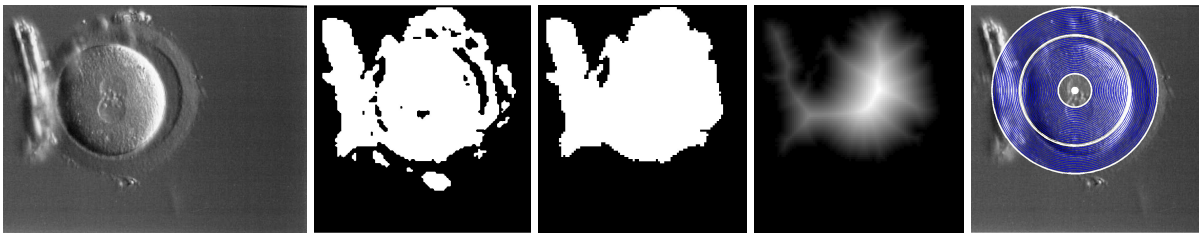

(a) (b) (c) (d) (e)

Figure 4: Approximate localization of the cell center. (a): original image. (b): binary mask obtained after thresholding the modulo of the gradient. (c): largest connected component with holes filled. (d): distance transform. (e) the maximum of the distance transform is considered as the approximate center of the cell. Note that the large artifact on the left does not significantly displace the maximum of the distance transform.

bilinear interpolation to an image J_i in polar coordinates:

$$\begin{aligned} J_i(\theta,\rho) &= I_i\left(c_x+\rho\cos(\theta), c_y+\rho\sin(\theta)\right) \\ 0\le\theta<2\pi \qquad \rho'\le\rho\le\rho'' \qquad i&=1\cdots N. \end{aligned} \tag{2}$$

In order to account for variations in the cell shape and errors in the centroid location, the range $[\rho' \div \rho'']$ of ρ values is very conservatively set to $[0.3r, 1.5r]$, where r represents the expected cell radius; this is a quite large range (see Figure 4e), which allows for large variations in the actual radius of the zygote, and for displacements of the estimated centroid (c_x, c_y). ρ and θ values are uniformly sampled in ρ_n and θ_n intervals, respectively, which correspond to rows and columns of each image J_i. We use $\rho_n = 80$, $\theta_n = 180$ in the following.

4.2.2 Computation of Energies

Images J_i are then processed in order to associate an energy to each pixel for each of the N planes. Such energy will drive the following graph-based formulation. Let α be the direction of apparent lighting due to HMC, which only depends on the optical setup and can be assumed known in most scenarios (if it's not, it can be easily estimated); we define an energy E_i for each pixel of J_i, regardless on its plane in the stack, as:

$$\begin{aligned} E_i(\theta,\rho) &= P\left(\overbrace{\cos(\theta-\alpha)\cdot G_\rho(J_i)}+\right. \\ &\qquad \left.\overbrace{\sin^2(\theta-\alpha)\cdot\left|G_\rho(J_i)\right|}\right) \end{aligned} \tag{3}$$

$$P(x) = \left(1+e^{\frac{x}{k}}\right)^{-1} \tag{4}$$

where G_ρ denotes the gradient operator along the ρ axis, and $P(\cdots)$ is a simple decreasing sigmoid function which conditions the energy values to lie in the $[0 \div 1]$ interval; the scaling parameter k is not critical, and can be safely set to $1/5$ of the image's dynamic range.

The first term in (3) dominates where the contour is orthogonal to the apparent light direction, i.e. where the cell is expected to appear significantly lighter ($\theta-\alpha\simeq 0$) or darker ($\theta-\alpha\simeq\pm\pi$) than the surroundings; large gradient values with a sign consistent with this assumption lead to lower energies. The second term takes account for the unpredictability of the contour appearance where the contour is parallel to the apparent light direction, and just associates lower energies to large absolute values for $G_\rho(J_i)$.

4.2.3 Building of a Directed Acyclic Graph

A single directed acyclic graph is built over the stack of all J_i images, by instantiating a node for each pixel and for each plane (for a total of $\rho_n \cdot \theta_n \cdot N$ nodes). Moreover:

- arcs are added connecting each node to its three 8-neighbors at the right on the same plane;
- every β_n columns, a set of *interfocal* arcs are added. In particular,

The cost of each arc is set to the energy $E_i(\theta,\rho)$ of its source node.

A single global source node s is added, with zero-cost arcs that lead to every pixel in the first column of every plane; also, we add a sink node reached by zero-cost arcs from every pixel at the last column of every plane.

4.2.4 Minimum-Cost Path

As the resulting graph is a directed acyclic graph, efficient algorithms are available for computing the minimum-cost path from the source node to the sink node. Such path passes through low-energy arcs, and is constrained by the graph topology to have a quite regular shape, because:

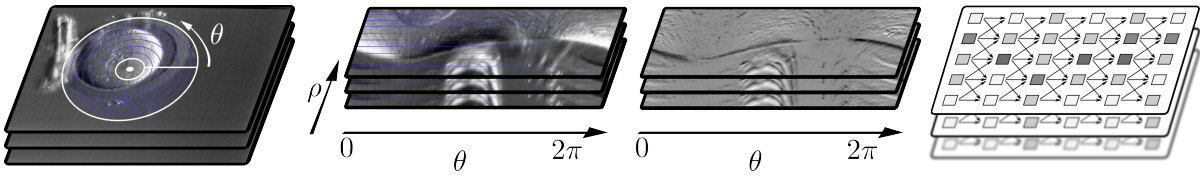

Figure 5: The stack of I_i slices (a) is transformed to J_i slices in polar coordinates (b), then an energy value E_i (c) is computed for each pixel and a graph is built on each (d). A single global graph is then computed.

- the path is forced to steadily move from left to right (i.e. increasing θ values);
- variations along the radial direction ρ are bounded in slope;
- shifts to an adjacent focal plane can only occur rarely (e.g. every β_n columns).

After excluding the source and sink nodes (which have no geometric meaning), the path can be brought back to cartesian coordinates by using the inverse transform to (2): the result is a curve in the (x,y,z) space. If the first and last nodes of the path (almost) match, the curve can be smoothly closed. If such points do not match, we have a strong hint that the image did not contain a zygote, or that the approximate center was very displaced with respect to the true center of the zygote; we are currently disregarding this possibility as none of our test images exhibits this issue, although we plan to investigate the related problem of the zygote *detection* in future works.

In practice, the resulting path estimates the 3D contour generating curve Γ. It simultaneously represents the contour of the cell and identifies its main focal plane: the interior of the resulting polygon projected to the 2D plane (x,y) defines the computed binary mask M. The average value for the focus plane associated to the nodes in the minimum-cost path defines the focus plane z_m where the cell contour is sharpest.

Larger values for ratio θ_n/ρ_n, as well as a smaller β_n parameter, allow more freedom to the path built over the graph, which translates to better accommodation of an irregular cell shape or a displaced centroid (c_x,c_y); at the same time, this reduces the robustness of the approach, as shape priors are less strongly enforced. We found any ratio between 1.5 and 3.0 to be acceptable, although we keep with $\theta_n/\rho_n = 180/80 = 2.25$ in the following; changing β_n has little effect in most cases, and should be set such that the ratio θ_n/β_n is larger than 8 – i.e. there are at least 8 places in the graph where the interfocal arcs are created – which allows the resulting contour generator curve to span at most 4 adjacent focal planes. Due to the almost spherical shape of the zygotes, none of our test images required a larger variation[4].

5 EXPERIMENTAL RESULTS

We evaluated the technique on 101 image stacks representing 84 unique zygotes from 22 different patients (some zygotes are acquired twice). Stacks are acquired with a 0.35 megapixel JVC camera attached to an Olympus IX-51 inverted microscope equipped with a 20x objective, HMC optics, and a 0.63x camera adapter. Each stack is composed by 23 images, acquired in a rapid sequence (10 frames per second) during a regular motion of the focus knob; due to the manual nature of the stack acquisition, the spacing between adjacent slices of a stack is not exactly fixed[5], but consistently averages between 8 and 12 microns; the whole stack covers approximately 200 microns, which amounts at twice the expected diameter of the cell. The contour generator curve Γ of the cell is always included in the range of focus, although not in a predictable position. The cell is always completely included in the image, but is not well centered in the image as the biologist acquiring the images uses the microscope oculars and thus does not have a reference for the center of the image acquired by the camera.

We can now quantitatively evaluate the effectiveness of our focusing technique. We compare z_m, the average focus plane of Γ determined by our algorithm, to a reference focus depth z_{ref}, obtained by an operator carefully navigating the stack and choosing the slice maximizing the overall contrast and precision of the cell contour. We consider z_{ref} as the ground truth.

We also compare two additional estimators for z_{ref}:

- z_{quick}, obtained by an operator rapidly focusing a stack (in about 2 seconds on average) by means

[4] note that if the cells were perfectly spherical then Γ would lie on a single focal plane

[5] note that fixed spacing is never assumed in our approach; still, equally-spaced slices, which we plan to acquire by means of automated microscopes, will prove very useful for performing 3D measurements on the resulting stacks

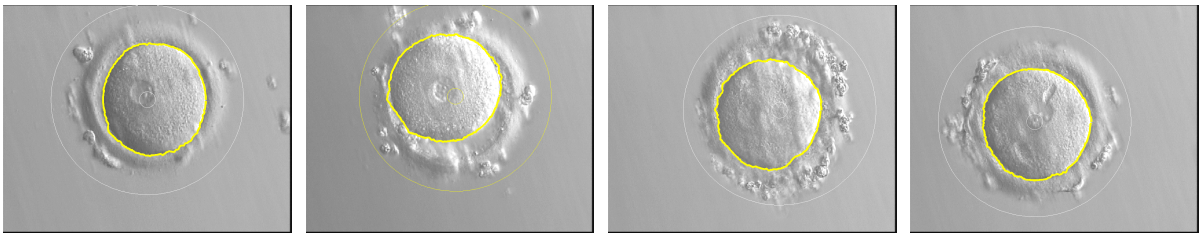

(a) (b) (c) (d)

Figure 6: Some images focused and simultaneously segmented by our approach. γ shown in yellow. Thin white lines delimit the circular corona around the detected approximate center (c_x, c_y).

Table 1: Evaluation of focusing performance (see main text). First row reports the error in terms of number of z-stack slices; second row expresses the approximate value in μm, assuming a fixed distance between adjacent slices of $10\mu m$.

	z_m	z_{quick}	$z_{\text{autofocus}}$
RMSE [slices]	1.26	3.22	3.90
RMSE [μm]	12.6	32.2	39.0

Table 2: Evaluation of segmentation performance (see main text).

q	d_a		d_m		e_a	e_e
	pixels	fraction of R	pixels	fraction of R		
0.949	2.625	0.020	5.823	0.044	0.017	0.077

of the mouse wheel, with the goal of getting an acceptable contrast.

- $z_{\text{autofocus}}$, the measure computed by the naive autofocusing algorithm which maximizes the average modulo of the gradient in the image; we use such measure in order to find the approximate cell center (see Section 4.1). We evaluated other simple histogram-based autofocusing algorithms, which performed consistently worse.

The root mean squared error (RMSE) with respect to z_{ref}, computed on all 101 stacks, is reported in Table 1 for each of z_m, z_{quick}, and $z_{\text{autofocus}}$.

On average, the contour generator curve spanned a range of 1.71 slices ($\approxeq 17\mu m$).

In order to evaluate the quality of the segmentation, we randomly selected 40 of the 101 stacks and created a ground truth binary mask T for each, by considering the slice with best focus as returned by our algorithm and manually segmenting the contour of the zygote on such slice. We then compared this ground truth value to the segmentation returned by algorithm, represented by a binary mask M, by considering:

- the Jaccard quality metric $q = \frac{|T \cap M|}{|T \cup M|}$ $0 \leq q \leq 1$, which approaches 1 for better segmentations;
- the average distance d_a and maximum distance d_m between the true boundary and the computed one;
- the relative error in the measured area e_a;
- the absolute error in the measured eccentricity e_e.

The results, shown in Table 2, are consistent with those reported in (Giusti et al., 2009), where a simplified version of the same algorithm is applied to one single image with the contour in good focus.

6 DISCUSSION, CONCLUSIONS AND RELATED WORKS

We presented an effective technique for simultaneously focusing an human zygote cell and recovering its contour. We maintain that, in this scenario, the problem of precise and repeatable focusing is strictly tied to the segmentation problem, as low-level focus measures which consider the image as a whole are easily misled by additional structures and debris which exhibit strong contrast. Our approach segments the cell and determines its focal plane in a single step, by operating on a single graph summarizing information from all the slices in the stack.

We have shown that our focusing algorithm is able to determine a repeatable focal plane, which has a

meaningful interpretation as the average depth of the contour generator curve of the cell. The precise and automated measurement of such depth is a fundamental step for providing accurate and repeatable measures of the zygote morphology which also account for 3D information. Obviously, this requires operating on stacks whose slices have a known depth, which we are going to obtain in the future. We are currently improving the system by automatically segmenting, measuring and locating in 3D other zygote structures such as the pronuclei. This has important applications in the clinical practice for In Vitro Fertilization.

REFERENCES

Beuchat, A., Thévenaz, P., Unser, M., Ebner, T., Senn, A., Urner, F., Germond, M., and Sorzano, C. (2008). Quantitative morphometrical characterization of human pronuclear zygotes. *Human Reproduction*, 23:1983–1992.

Gianaroli, L., Magli, M. C., Ferraretti, A. P., Lappi, M., Borghi, E., and Ermini, B. (2007). Oocyte euploidy, pronuclear zygote morphology and embryo chromosomal complement. *Human Reproduction*, 22(1).

Giusti, A., Corani, G., Gambardella, L., Magli, C., and Gianaroli, L. (2009). Segmentation of human zygotes in hoffman modulation contrast images. In *Proc. of MIUA*.

Karlsson, A., Overgaard, N. C., and Heyden, A. (2005). *Scale Space and PDE Methods in Computer Vision*, chapter A Two-Step Area Based Method for Automatic Tight Segmentation of Zona Pellucida in HMC Images of Human Embryos, pages 503–514. Springer.

Kuijper, A. and Heise, B. (2008). An automatic cell segmentation method for differential interference contrast microscopy. In *Proceedings of ICPR*.

Morales, D., Bengoetxea, E., and Larrañaga, P. (2008). Automatic segmentation of zona pellucida in human embryo images applying an active contour model. In *Proc. of MIUA*.

Shih, L. (2007). Autofocus survey: a comparison of algorithms. *Digital Photography*.

Soille, L. and Vincent, P. (1991). Watersheds in digital spaces: an efficient algorithm based onimmersion simulations. *IEEE Transactions on Pattern Analysis and Machine Intelligence*.

Xu, C. (1998). Snakes, shapes, and gradient vector flow. *IEEE Transactions on Image Processing*.

Zabih, R. and Kolmogorov, V. (2004). Spatially coherent clustering using graph cuts. In *Proc. of CVPR*.